JMEPEG (2005) 14:85-90
DOI: 10.1361/10599490522356

1059-9495/$19.00

# Effect of Small Strain Levels on Special Boundary Distribution in Commercially Pure Nickel

*B. Guyot, S.-L. Lee, and N.L. Richards*

*(Submitted August 3, 2004)*

**Commercially pure nickel has been processed via low-strain and high-strain routes using various thermomechanical cycles with isochronal annealing from 500 to 900 °C. Electron backscattered diffraction was used to characterize the percentage of special boundaries (Σ3-29) formed. Measurements also included twin variants based on Σ3″. Of the various single-strain and multiple-strain temperature combinations that were processed, both routes showed that a single low strain of about 2 to 6% followed by annealing at 900 °C for 10 min resulted in a doubling of the special fraction of grain boundaries. In addition, the Σ3″ variants were also approximately doubled without the recourse to multiple processing and/or multiple heat treatments. It was proposed, based on theories from the literature, that extrinsic grain boundary dislocations formed at low strain levels in a mantle-core formation and, on annealing, climbed along the boundary and formed special grain boundary types.**

**Keywords** annealing, cold working, electron backscattered diffraction analysis, metallography, nickel

## 1. Introduction

In recent research the manipulation of the grain boundary character of commercially pure nickel was attempted using two processing routes involving low and high strain levels as part of various thermomechanical cycles. One process (route 1), concentrated on single and multiple processing routes at strain levels from 3 to 12% cold work, followed by annealing at temperatures from 500 to 900 °C. The other route (route 2) used single and multiple strain levels from 2.5 to 25% strain per cycle followed by annealing at temperatures from 500 to 900 °C. The above processing routes are in line with the general division of processing promulgated by Thomas and Randle (Ref 1) and by Schwartz et al. (Ref 2) for low strain levels, and also that of Palumbo (Ref 3) using the high-strain, multiple-processing route.

Thomas and Randle (Ref 1), using commercially pure nickel, have shown that low strain levels of about 6%, combined with extensive annealing for up to 24 h, is capable of increasing the twinning frequency from 15.3 to 39.8% using multiple annealing cycles at temperatures from 500 to 1000 °C for times from 20 min to 24 h. King and Schwartz (Ref 4), working on pure copper, have also established processing routes similar to those of Randle (Ref 1) using 6% strain and, again, similar multiple temperature-time combinations.

Palumbo (Ref 3), on the other hand, has promoted the use of deformation levels from 5 to 30%, combined with multiple strain annealing with three to seven cycles, and with matrix recrystallization being necessary. In alloy 625, for example, multiple processing resulted in special boundary levels increasing from 24.8 to 70.7%.

It is clear from the literature that both the single-step strain anneal and the multiple-strain recrystallization methods are capable of increasing the percentages of special boundaries compared with baseline values. Justification, however, for choosing one of the two main routes and the various strain/temperature/time combinations remains unclear. To evaluate the key process parameters for the two processing routes, two separate projects were undertaken by Lee (Ref 5) and Guyot (Ref 6) using commercially pure nickel to eliminate the effects of precipitation hardening and solute effects associated with nickel (Ni)-base superalloys. The present article is strictly concerned, however, with communicating an interesting and potentially commercially significant result that can be achieved by both processing routes. Both routes, utilizing a simple single-stage strain followed by annealing for 10 min in the temperature range 800 to 900 °C, resulted in doubling the proportion of special boundaries (Σ3-29) without either long-term annealing and/or without multiple processing. In addition, the $\Sigma 3^n$ special boundary content was also doubled.

## 2. Experimental

Commercially pure Ni sheets, 3 mm thick, in the mill-annealed condition (composition shown in Table 1) were used for processing. For the low-strain processing (route 1), deformation was accomplished by room-temperature straining tensile test pieces to the ASTM E 8 specification. The deformation levels ranged from 3 to 12%. Annealing was carried out at temperatures between 500 and 900 °C in flowing argon (Ar) to minimize oxidation. The 2.5 to 25% strain samples were

**Table 1 Chemical composition of commercially pure Ni**

| Composition, wt.% | | | | |
|---|---|---|---|---|
| **Ni** | **Mn** | **Fe** | **Cu** | **Ti** |
| bal | 0.18 | 0.021 | 0.052 | 0.023 |

**B. Guyot,** NRC Institute for Aerospace Research (NRC-IAR), 5145 Decelles Ave., Campus Université de Montréal, Montréal, Quebec, Canada, H4T 1W5; **S.-L. Lee,** and **N.L. Richards,** Department of Mechanical & Manufacturing Engineering, University of Manitoba, Winnipeg, MB, Canada, R3T 5V6. Contact e-mail: nrichar@cc.umanitoba.ca.

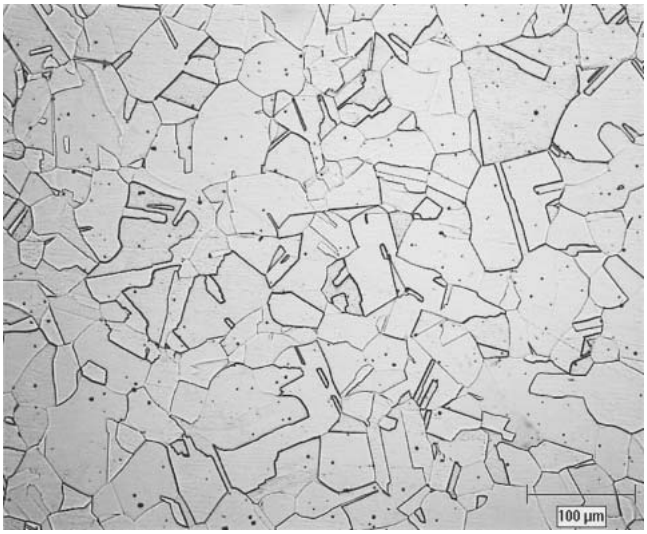


**Fig. 1** Optical micrograph of as-received commercially pure Ni

cold rolled on a 203 mm (8 in.) laboratory mill with lubrication and were annealed at temperatures between 500 and 900 °C, with both routes using an isochronous annealing time of 10 min at temperature.

Metallographic preparation for orientation image microscopy (OIM) was carried out using conventional methods with the final polish using 0.05 μm γ-alumina. OIM analysis was performed on a JEOL 5900 (Peabody, MA) scanning electron microscope using TSL (EDAX, Makwak, NJ) version 3.5 software. Some 200 to 300 grains were analyzed for each sample, with special boundaries, $\Sigma_{sp}$, being defined as those from Σ(3-29). For the measurement of 200 to 300 grains, the fractional standard error from Alexandereanu and Was (Ref 7) was estimated to be between 0.05 and 0.1. Confidence index values were in the range of approximately 0.5 to 0.8, well above the 0.1 value determined by TSL software to give 95% confidence in the data. OIM measurements were made along the center portion of the test samples.

Hardness measurements for route 1 were carried out using a conventional Vickers hardness tester, while those for route 2 used a microhardness tester with the 100 g load and a diamond indenter.

## 3. Results

### 3.1 Metallography

The as-received microstructure (Fig. 1) consisted of austenite grains with some directionality in the microstructure and evidence of twinning. Measurements of grain size were made manually using the linear intercept method, yielding a grain size of 28 μm longitudinally, with respect to the rolling direction, and 25 μm in the transverse direction.

### 3.2 Hardness versus Strain and Annealing Temperature for Commercially Pure (CP) Ni

Figure 2(a) and (b) show the effect of single cold-working stages and annealing on hardness. In the low-strain samples, sufficient recovery of hardness did not occur until about 800 to 900 °C at >3% strain, while in the high-strain regimen greater

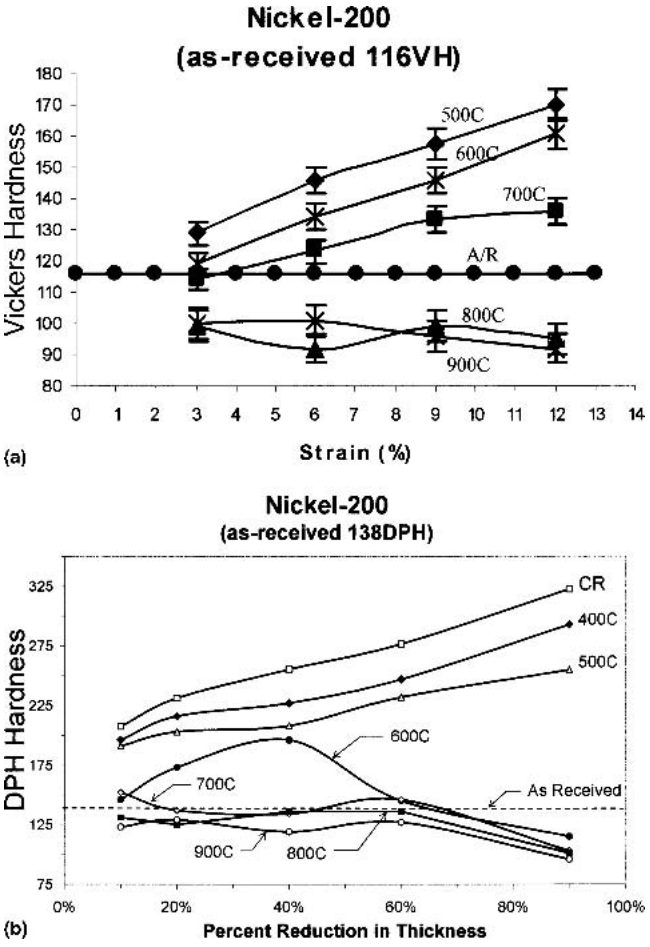


**Fig. 2** Hardness-strain curves at various annealing temperatures

than ~40% strain at 600 °C was needed for the slope of the hardness/percentage reduction in thickness relationship to fall.

### 3.3 Electron Backscattered Diffraction Analysis

Electron backscattered diffraction analysis of the as-received material (Table 2, Fig. 3a) shows the presence of 26.3% of Σ3 boundaries, 2.1% of Σ9 boundaries, and 0.6% of Σ27 boundaries, with a total Σ from (3-29) of 34.9%. Figure 3(b), on the other hand, shows only the non-coincidence site lattice random boundaries (more than Σ29), with rotation angles >15°. These are boundaries with the potential for a continuous path for crack propagation.

Single levels of straining from 3 to 12% and annealing from 500 to 900 °C for 10 min gave the $\Sigma_{sp}$ values shown in Table 2. The highest values were achieved using a single 6% strain and annealing at 900 °C for 10 min increasing the $\Sigma_{sp}$ from the as-received values given earlier to 74.7% (Σ3, 60.3%; Σ9, 8.3%; and Σ27, 4.2%), which is more than double the as-received material value. Figure 4(a) shows an OIM image from the single-step (6%)/900 °C, 10 min sample, with $\Sigma_{sp}$ boundaries coded gray and random boundaries coded black. Similarly, Fig. 4(b) shows only the random (Σ > 29) boundaries. As can be seen from Fig. 4(b), compared with the as-received random boundary network in Fig. 3(b), the special processing has broken up the connectivity of the high angle-boundary

**Table 2 Percentage special boundaries and grain size from route 1 processing**

| Temperature °C | Processing(a), % | Grain size, μm | % Σ3 | % Σ9 | % Σ27 | Total % $\Sigma_{sp}$ |
|---|---|---|---|---|---|---|
| … | As received | 28.0 L; 25.0 X | 26.1 | 2.1 | 0.6 | 34.9 |
| 500 | 1-3 | 27.0 L; 24.0 X | 27.8 | 2.5 | 0.2 | 32.3 |
| | 1-6 | 25.0 L; 21.4 X | 23.6 | 1.8 | 0.5 | 29.2 |
| | 1-12 | 23.0 L; 22.0 X | 25.3 | 1.7 | 1.0 | 29.6 |
| 700 | 1-3 | 28.8 L; 23.1 X | 24.3 | 1.4 | 0.3 | 28.1 |
| | 1-6 | 25.4 L; 21.3 X | 33.4 | 1.3 | 0.5 | 41.5 |
| | 1-12 | 29 L; 23.7 X | 25.3 | 1.4 | 0.2 | 29.5 |
| 800 | 1-3 | 29 L | 30.7 | 2.5 | 0.3 | 36.6 |
| | 1-6 | 50 L | 27.3 | 2.4 | 1.1 | 31.6 |
| | 1-12 | 53 L | 28.0 | 3.1 | 0.1 | 33.1 |
| 900 | 1-3 | 69 L | 33.0 | 1.2 | 1.3 | 37.0 |
| | 1-6 | 60 L | 60.3 | 8.3 | 4.2 | 74.7 |
| | 1-12 | 55 L | 47.5 | 4.3 | 2.6 | 58.1 |

Note: L, length; X, width. (a) Ten minutes at temperature

network, which has been shown to be beneficial to properties (Ref 8, 9). Note that Fig. 4(b) shows only the random grain-boundary network and should not be confused with the grain size developed during processing.

Route 2 processing gave the $\Sigma_{sp}$ values shown in Table 3. Again, strain values from 2.5 to 10% per cycle gave the highest special fraction of grain boundaries from 46.3 to 65% (Fig. 5a-d) compared with the as-received value of 34.9%, and the minimum value of 4.8% processed at 25% strain and annealed at 600 °C. The $\Sigma 3^n$ values were again approximately double the as-received values.

### 3.4 Grain Size Data

The effects of processing on grain size for route 1 are also shown in Table 2. Up to about 700 °C, the grain size is reasonably stable in the range 23 to 31 μm, with some anisotropy in grain size evident up to 800 °C. Processing at 800 °C and greater than ~6% strain, however, resulted in an increase in grain size up to 50 μm and subsequently, with higher temperature, to nearly 70 μm. Thomas and Randle (Ref 1) have shown in CP Ni at low strain levels, 6% in their case, temperatures >850 °C are necessary to activate grain boundary migration and subsequent grain growth. The present results would appear to support their analysis.

For route 2 processing, the grain size data (Table 3) show some slight directionality for some samples due to the higher strain levels during rolling. Generally, the anisotropy was minor except for the 1 × 25% sample annealed at 600 °C.

It should be noted that the grain boundary plane was not considered in the present research, but, as pointed out by Hassold et al. (Ref 10), elimination of the boundary plane requirements would not increase the special fraction of boundaries during grain growth. In addition, Hassold et el. (Ref 10) also pointed out that during grain growth the boundary plane would vary with the movement of the boundary and should not significantly influence the special fraction of boundaries during annealing.

## 4. Discussion

It is clear from the literature that careful processing with respect to strain, temperature, and time can significantly increase the fraction of special boundaries in metals. What is not clear from a fundamental point of view, however, are the reasons for the multiple strain/temperature processing levels advocated for the low-strain and high-strain routes. The following analysis, based on a combination of several theories available in the literature, attempts to explain the basis for the low-strain behavior in terms of the accumulation of inhomogeneous distributions of dislocations during straining and their annihilation during annealing.

During straining, Thompson et al. (Ref 11) have shown that inhomogeneous deformation occurs in the immediate area of grain boundaries, leading to a concept of a harder "mantle" adjacent to the boundary and a softer "core" in the grain interior. In addition, it has been known for some time (Ref 12) that grain boundaries can act as sources for dislocations. Murr (Ref 13) has conclusively shown that grain boundary ledges act as sources for dislocations during straining. Thus, besides the intrinsic (equilibrium) grain boundary dislocations, extrinsic grain boundary dislocations (EGBDs) are formed during straining, leading to the mantle of geometrically necessary dislocations adjacent to the grain boundary.

Meyers and Ashworth (Ref 14) also have shown in the grain boundary that shear stresses can exist that are up to three times higher than the homogeneously applied stresses on the grain overall. Thus, dislocation emission would likely occur at grain boundary ledges, before initiation in the grain interior. Furthermore, the grain boundary emission of extrinsic dislocations reduces the stress concentration for the generation of geometrically necessary dislocations, which accommodate these stresses. The grain boundary flow stress is, therefore, greater than the bulk value, which is the basis of the mantle-and-core proposal of Thompson et al. (Ref 11). On further straining, the elastic strained region becomes plastic and conventional macroscopic strain occurs. In this case, dislocations in the mantle and core will behave in a similar fashion, and the flow stress in both the grain boundary and core will become similar.

The present research has shown that 2.5 to 6% strain gives the highest $\Sigma_{sp}$ values. It is, therefore, proposed that strain levels of ~2.5 to 6% produce the mantle-core effect, whereas greater strains such as 9 and 12% result in the flow stress of the core and mantle being approximately the same. That is, dislocations have spread throughout the grains. Thus, at low

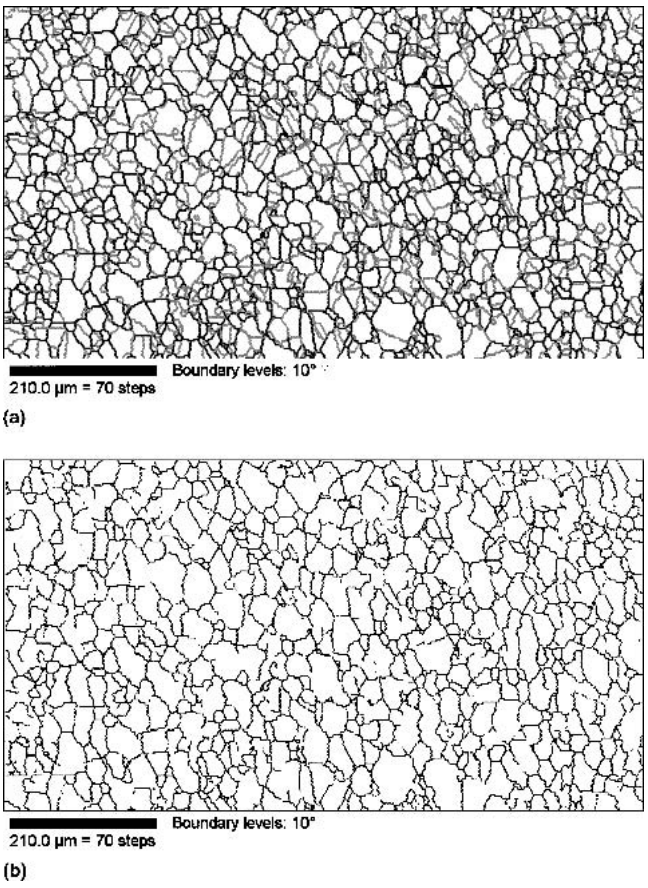


**Fig. 3** (a) OIM image of as-received material: gray lines are Σ(3-29) and black lines are random boundaries; and (b) random grain boundary network: Σ > 29

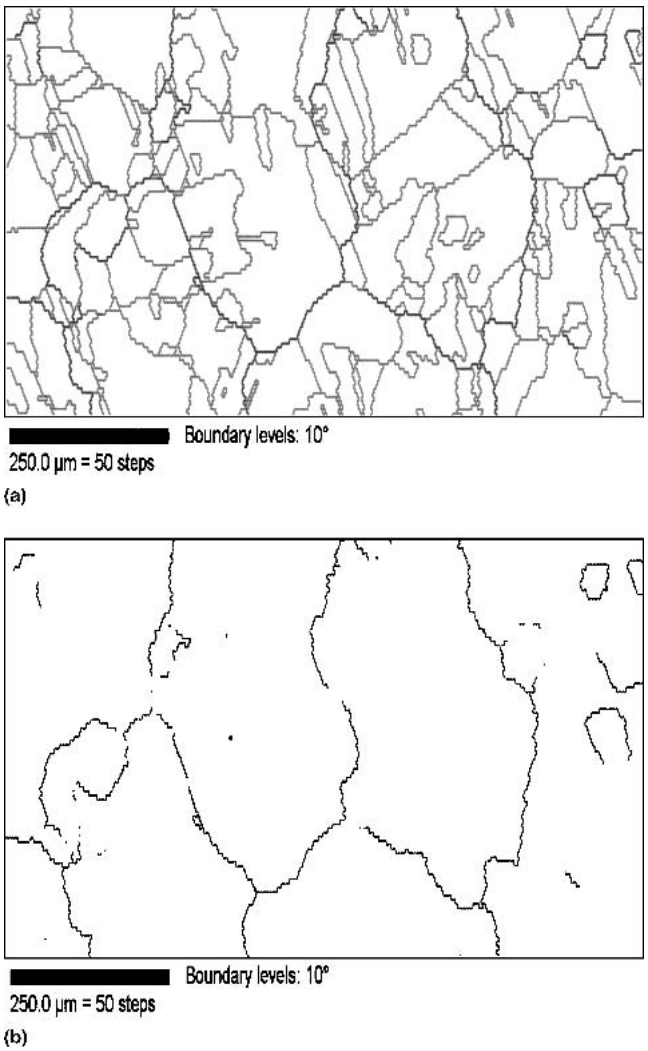


**Fig. 4** OIM maps for one-step 6% strain at 900 °C: (a) special grain boundaries are shown with gray lines equivalent to Σ(3-29) and black lines equivalent to random boundaries; and (b) only random boundaries: Σ > 29

strains recrystallization does not occur, whereas at higher strain levels, depending on temperature, recrystallization may occur and new high-angle grain boundaries form, destroying the existing microstructure, which is conducive to the formation of special boundaries.

Sangal and Tangri (Ref 15) have shown that, during annealing, the nonequilibrium grain boundaries can be transferred to an equilibrium state via grain boundary migration, and the migration is related to dislocated annihilation in the area of the grain boundary. In the first stage, EGBD cores spread out into a number of partial dislocations, followed by a climb of these dislocations along the grain boundary plane toward the triple points. The annihilation of the EGBDs is a function of temperature and time and is given by (Ref 15):

$$\frac{1}{\rho}-\frac{1}{\rho_o}=\left\{\frac{DGV\left[1-2\ln\left(\frac{r_o}{L}\right)\right]}{L(1-\nu)\,kT\ln\left(\frac{R_o}{r_o}\right)}\right\}t \qquad \text{(Eq 1)}$$

where ρ is the instantaneous EGBD density, $\rho_o$ is the initial EGBD density, $D$ is the self-diffusion coefficient, $V$ is the atomic volume, $L$ is the length of grain boundary, $r_o$ is approximately equal to the Burger's vector, $R_o$ is approximately equal to the half distance between triple points, $G$ is the shear modulus, and $t$ is the time.

From Eq 1, the rate of EGBD annihilation, $d\rho/dt$, is a function of grain size, temperature, and instantaneous density (i.e., ρ of EGBDs). Also, the formation of increased levels of special boundaries resulting in twinning often results in segments of grain boundaries changing from random to special. Thus, twinning occurring across a grain is responsible for breaking up the random grain boundary structure with segments of low $\Sigma_{sp}$ interspersed between segments of random boundary structure. Therefore, a propagating crack running intergranularly would likely be stopped or deviated by the special boundaries, as shown in the research of Guo et al. (Ref 16), during the welding of Inconel 718. Grain boundary segments, as described above, were seen to be crack-free if they were of the $\Sigma_{sp}$ type (Σ3-29), but were cracked if they were of the random type (Σ > 29).

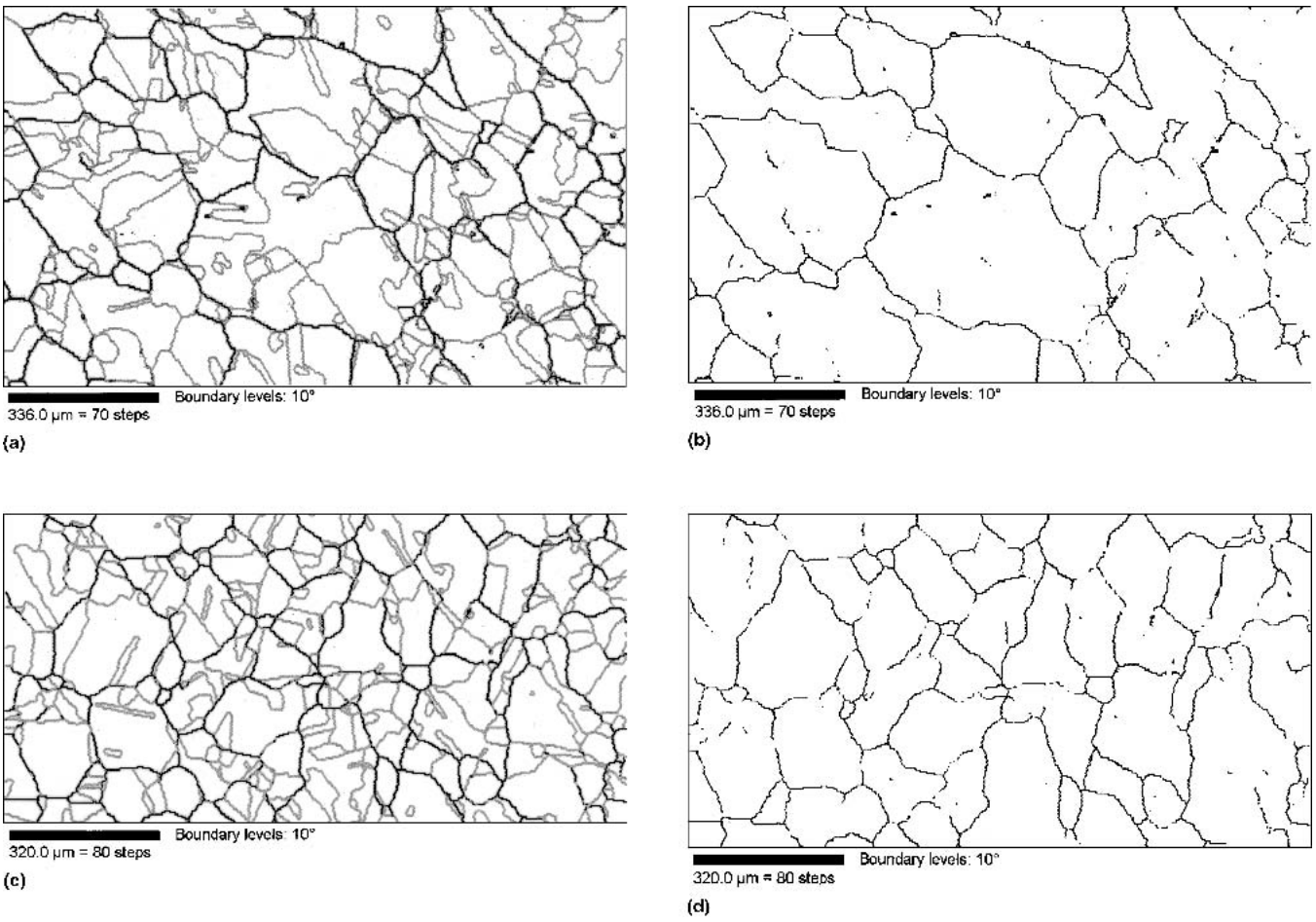


**Fig. 5** OIM images and random boundary images for 2.5 and 10%, one-step strain levels: gray lines are Σ(3-29), and black lines are random boundaries, Σ > 29: (a) 2.5% + 900 °C for all boundaries ($\Sigma_{sp}$ = 46%); (b) 2.5% + 900 °C random only; (c) 10% + 900 °C for all boundaries ($\Sigma_{sp}$ = 47%); and (d) 10% + 900 °C random only

**Table 3 Percentage special boundaries and grain size from route 2 processing**

| Processing(a) | % Σ3 | % Σ9 | % Σ27 | % $\Sigma_{sp}$ total | Grain size, µm |
|---|---|---|---|---|---|
| As received | 26.1 | 2.1 | 0.6 | 34.9 | 28.0 L; 25 X |
| 1 × 2.5%/900 °C | 37.4 | 5.6 | 0.8 | 46.3 | 62.3 L; 56.9 X |
| 1 × 5%/750 °C | 36.1 | 4.0 | 1.6 | 46.0 | 40.1 L; 37.9 X |
| 1 × 5%/900 °C | 50.2 | 8.1 | 3.0 | 65.0 | 63.1 L; 59.2 X |
| 1 × 10%/800 °C | 47.7 | 4.8 | 0.7 | 56.8 | 42.2 L; 40.1 X |
| 1 × 10%/900 °C | 38.0 | 5.2 | 0.9 | 46.6 | 59.2 L; 50.9 X |
| 1 × 18%/800 °C | 46.6 | 5.1 | 1.0 | 57.5 | 32.9 L; 28.2 X |
| 1 × 20%/750 °C | 36.4 | 4.4 | 0.1 | 46.6 | 32.6 L; 25.4 X |
| 1 × 20%/900 °C | 31.3 | 1.7 | 0.6 | 40.9 | 57.3 L; 51.2 X |
| 1 × 25%/600 °C | 2.4 | 0.3 | 0 | 4.8 | 50.0 L; 24.0 X |
| 1 × 25%/700 °C | 11.2 | 1.0 | 0.3 | 15.7 | 32.0 L; 27.2 X |
| 1 × 25%/800 °C | 24.7 | 2.0 | 0.6 | 29.5 | 30.9 L; 28.7 X |
| 1 × 25%/900 °C | 10.8 | 0.3 | 0.2 | 13.1 | 55.1 L & X |

Note: L, length; X, width. (a) Ten minutes at temperature

Further consideration of the effect of small strain levels on the formation of increased levels of $\Sigma_{sp}$ boundaries may be possible following the "fine-tuning" concept of Randle (Ref 8). Randle assumed that recrystallization in CP Ni does not occur at low strain levels, but that the local grain boundary crystallography can be modified by grain boundary rotation and recovery. This is in line with the present hypothesis (Fig. 2a) in which it can be seen that at 700 °C recovery mechanisms may operate but recrystallization does not occur. At 800 and 900 °C, however, the hardness data are less clear, in that the Vickers

pyramid Number (VPN) at high-percentage reductions is reduced to below the as-received values, as grain boundary migration and grain growth are likely occurring. In general, however, the accumulation of a sufficient dislocation density via low strain levels within the grain boundary region, without extensive recrystallization, appears to be beneficial in influencing the generation of grain boundary dislocation types that incorporate low $\Sigma$ elements. On the other hand, at high levels of strain, recrystallization is promoted and the accumulation of dislocation, which enhances low $\Sigma$ grain boundary formation, is minimized, or eliminated, depending on the actual percentage reduction/temperature/time combination.

In the case of the 700 °C samples, grain boundary recovery likely occurs as shown by Sangal and Tangri (Ref 15) in association with the proposal of Randle (Ref 8) for some rotation of the grain boundary plane. At 800 °C, the same mechanism may apply, accompanied by grain boundary migration and grain growth. At 900 °C, even at the low strains used, grain growth can occur, and the enhanced formation of annealing twins leads to $\Sigma_{sp}$ values of up to 76% via the growth accident model of Mahajan et al. (Ref 17) and Pande et al. (Ref 18). In this model, it is necessary for grain boundaries to migrate in line with the proposal of Sangal and Tangri (Ref 15), with the driving force being dependent on the grain boundary curvature (i.e., the smaller the radius of curvature, the greater the driving force). The equation of Pande et al. (Ref 18) for twin density is as follows (Ref 18):

$$\frac{p}{p_o} = \frac{D_o}{D} \log\left[\frac{D}{D_o}\right] \quad \text{(Eq 2)}$$

where $p$ is the twin density, and $p_o$ and $D$ are constants. In Eq 2, $p_o$ is proportional to the ratio of the average grain boundary to twin boundary energy. Thus, the twin density is only a function of grain size. As an illustration, using the present route 1 data from Table 2, the $\Sigma_{sp}$ values tend to increase with increasing grain size, which is in agreement with Eq 2 over a range from approximately 20 to 70 μm.

## 5. Conclusions

Using a combination of strain values from 2.5 to 25%, plus isochronal annealing of CP Ni at various temperatures, it has been shown that:

- Single processing routes have shown that strains in the range of 2 to 6%, combined with annealing, are capable of increasing the special fraction ($\Sigma$3-29) of grain boundaries from >35 to >70%.
- Analysis of the theories available in the literature shows that EGBDs, stored by straining in grain boundary regions, are, upon annealing, capable of forming special boundaries in the range $\Sigma$(3-29).
- Strain levels higher than ~6% (i.e., in the range 6-12%), combined with annealing, generally result in recrystallization and the elimination of the EGBDs responsible for low $\Sigma$ boundary formation.
- Increasing grain size to approximately 20 to 70 μm, due to increased annealing temperatures, resulted in an increase of the fraction of special boundaries, which is in agreement with Eq 2.


### Acknowledgments

The authors would like to recognize the assistance of technicians John van Dorp and Mike Boswick of the Department of Mechanical and Manufacturing at the University of Manitoba. Funding for the research of Lee and Guyot came from a Discovery Grant to Dr. Richards from the National Sciences and Engineering Council (NSERC), Ottawa, ON, Canada.


### References


1. C.B. Thomas and V. Randle, Fine Tuning at $\Sigma 3^n$ Boundaries in Nickel, *Acta Mater.,* Vol 45 (No. 12), 1997, p 4909-4916
2. A.J. Schwartz, M. Kumar, and W.E. King, Influence of Processing Method on the Grain Boundary Character Distribution and Network Connectivity, *Mat. Res. Soc. Symp. Proc.,* Vol 586, 2000, p 3-13
3. G. Palumbo, Metal Alloys Having Improved Resistance to Intergranular Stress Corrosion Cracks, U.S. Patent 5,817,193, Oct 6, 1998
4. W.E. King and A.M. Schwartz, Towards Optimization of the Grain Boundary Character Distribution in OFE Copper, *Scr. Mater.,* Vol 38 (No. 3), 1998, p 449-455
5. S.-L. Lee, "The Effects of Small Strains and Heat Treatment Processing on the Formation of Special Grain Boundaries in Commercially Pure Nickel," Master's thesis, University of Manitoba, 2003
6. B. Guyot, "Effect of Cold Working and Isochronal Annealing Processing Parameters on Special Grain Boundary Fractions in Commercial Purity Nickel," Master's thesis, University of Manitoba, 2003
7. B. Alexandereanu and G.S. Was, A Priori Determination of the Sampling Size for Grain-Boundary Character Distribution and Grain-Boundary Degradation Analysis, *Philos. Mag. A,* Vol 81 (No. 8), 2001, p 1951-1965
8. V. Randle, Grain Assemblage in Polycrystals, *Acta Mater.,* Vol 42 (No. 6), 1994, p 1769-1784
9. M. Kumar, W.E. King, and A.J. Schwartz, Modifications to the Microstructural Topology in FCC Materials Through Thermomechanical Processing, *Acta Mater.,* Vol 48 (No. 9), 2000, p 2081-2091
10. G.N. Hassold, E.A. Holm, and M.A. Miodownik, Accumulation of Coincidence Lattice Site Boundaries During Grain Growth, *Mater. Sci. Technol.,* Vol 19 (No. 6), 2003, p 683-687
11. A.W. Thompson, M.J. Baskes, and W.F. Flanagan, The Dependence of Polycrystal Work Hardening on Grain Size, *Acta Metall.,* Vol 21, 1973, p 1017-1028
12. J.C.M. Li, Petch Relationship and Grain Boundary Sources, *Trans. AIME,* Vol 227, 1963, p 239-247
13. L.E. Murr, Some Observations of Grain Boundary Ledges and Ledges as Dislocation Sources in Metals and Alloys, *Metall. Trans.,* Vol 6A, 1975, p 505-513
14. M.A. Meyers and E. Ashworth, A Model for the Effect of Grain Size on the Yield Stress of Metals, *Philos. Mag. A,* Vol 46 (No. 5), 1982, p 737-759
15. S. Sangal and K. Tangri, Effect of Small Plastic Deformation and Annealing on the Properties of Polycrystals: Part II. Theoretical Model for the Transformation on Non-Equilibrium Grain Boundaries, *Metall. Trans.,* Vol 20A (No. 3), 1989, p 479-489
16. H. Guo, M.S. Chaturvedi, and N.L. Richards, Effect of the Nature of Grain Boundaries on Intergranular Liquation During Welding of a Nickel Base Alloy, *Sci. Technol. Weld.,* Vol 3 (No. 5), 1998, p 257-259
17. S. Mahajan, C.S. Pande, M.A. Imam, and B.B. Rath, Formation of Annealing Twins in fcc Crystals, *Acta Mater.,* Vol 45 (No. 6), 1997, p 2633-2638
18. C.S. Pande, M.A. Imam, and B.B. Rath, Study of Annealing Twins in FCC Metals and Alloys, *Metall. Mater. Trans.,* Vol 21A, 1990, p 2891-2896